Collados-Lara Antonio-Juan (Orcid ID: 0000-0002-5693-2048)

Intra-day variability of temperature and its near-surface gradient with elevation over mountainous terrain: comparing MODIS Land Surface Temperature data with coarse and fine scale near-surface measurements

Antonio-Juan Collados-Lara[1,2,3 *], Steven R. Fassnacht[2, 3, 4], David Pulido-Velazquez[1,5], Anna K.D. Pfohl[3,6], Enrique Morán-Tejeda[2,3,7], Niah B.H. Venable[2,3], Eulogio Pardo-Igúzquiza[1], and Kira Puntenney-Desmond[3]

1 Instituto Geológico y Minero de España, Ríos Rosas 23, 28003 Madrid, España
2 ESS-Watershed Science, Colorado State University, Fort Collins, CO 80523-1476, USA
3 Natural Resources Ecology Laboratory, Fort Collins, CO 80523-1499, USA
4 Cooperative Institute for Research in the Atmosphere, Fort Collins, CO 80523-1375, USA
5 Universidad Católica de Murcia, Campus de los Jerónimos s/n, 30107 Guadalupe, Murcia, España
6 Geosciences, Colorado State University, Fort Collins, CO 80523-1482, USA
7 Departamento de Geografía, Universidad de las Islas Baleares, Carretera de Valldemossa km 7.5, 07122 Palma, España

* Corresponding author

E-mail addresses: ajcollados@gmail.com

This is the author manuscript accepted for publication and has undergone full peer review but has not been through the copyediting, typesetting, pagination and proofreading process, which may lead to differences between this version and the Version of Record. Please cite this article as doi: 10.1002/joc.6778

Abstract

Where land surface air temperature data are not available, satellite land surface temperature are used. However, the coarse spatial resolution of satellite-derived products may yield errors at the local scale. This work shows the differences between the MODIS Land Surface Temperature and Emissivity (MOD11A1) product and ground measurements at two different scales. We used data from 21 SNOTEL stations across the northern Front Range of Colorado to represent the coarse scale and 17 iButton temperature sensors across the Colorado State University Mountain Campus to represent the fine scale. We found significant differences in the temperature and its changes with elevation for the two spatial scales. At the fine scale, cold air drainage can induce an inversion of the temperature gradient with elevation. A higher correlation was found during the nighttime at the fine scale, while, at the coarse scale, higher correlations were observed during the daytime. On windy nights, temperatures do not cool as much as on calmer nights, and the coarse scale near-surface temperature gradient with elevation persists, though the fine scale inversions do not develop. The near-surface temperature gradients with elevation based on the MODIS pixels are similar to the ground-based data at the coarse scale but not at the fine scale. Thus, one must be cautious in selecting the near-surface temperature gradients with elevation for mountainous terrain when different scales are considered, and a proper validation of satellite products is necessary prior to their use to avoid the propagation of uncertainties.

Keywords: temperature variability, near-surface temperature gradients with elevation, temperature correlation with elevation, cold air drainage, iButton sensors, SNOTEL stations, MODIS LST

1. Introduction

The large spatial variability of climatic variables has an important influence on hydrological processes. In the literature, studies have analyzed the spatiotemporal distribution of precipitation and temperature (Monestiez et al., 2001; Bayat et al., 2013) that illustrate important variability of these data with elevation. Many hydrological processes (e.g. evapotranspiration, snow accumulation or snowmelt) are driven by air temperature, amongst other meteorological variables. Air temperature is influenced by various land and atmospheric conditions and can have an important variability due to spatiotemporal changes in the governing conditions (Pape and Löffler, 2004). Therefore, a chosen hydrological analysis approach can be sensitive to the selection of the spatiotemporal resolution considered in a study. Broad temperature patterns are studied through point measurements obtained from meteorological or hydrometeorological stations that tend to be coarsely spaced due to technical or financial limitations, especially in areas of sparse populations (Shiklomanov et al., 2002; Venable et al., 2015; Fassnacht et al., 2018). However, in recent years, smaller and less expensive temperature sensors (e.g. Hobo, Stowaway Tidbit, Thermochron iButton, Blue Maestro) have become popular (Irvine et al., 2017; Navarro-Serrano et al., 2019).

The Land Surface Temperature (LST) data obtained from satellites constitute another source of information, especially where temperature data are limited. Satellite LST is the radiative skin temperature of the land surface measured in the direction of the satellite. MODIS and AVHRR LST products have twice-daily temporal resolution and have been employed in hydrological studies (Wang et al., 2009; Khorchani et al, 2018). However, the spatial resolution of these products (1 and 1.1 km, respectively) may not be adequate where a finer spatial scale resolution is necessary to capture the temperature patterns, such as areas with cold air drainage (Bergen, 1969; Hubbart et al., 2007; Bigg et al., 2014).

Daily and monthly data are commonly employed to address hydrological questions (Hannah et al., 2011), and the distribution of meteorological variables are modeled from different orographic or landscape patterns using these different temporal resolutions (Benavides et al., 2007; Collados-Lara et al., 2018). Hydrological models incorporate temperature at the basin scale for lumped approaches (Jodar et al., 2018) to the kilometer scale for distributed approaches (Collados-Lara et al., 2019). Sometimes these resolutions are adequate for hydrological assessment, but other cases require finer resolutions (temporal and spatial) to assess the availability of water resources (Young et al., 2009; Chen et al., 2019). These are often not available or are not well distributed at the necessary resolution. In these cases, we use information generated from other sources, such as well-known patterns (e.g. near-surface temperature gradient with elevation (NSTGE)) for specific case studies (Hudson and Wackernagel, 1994) or remote sensing LST (Zhang et al., 2014).

Terrain parameters, in particular elevation at a relatively coarse scale, and slope and aspect at a finer scale, are used to estimate the spatial distribution of temperature. In the lower layers of the atmosphere, the free atmospheric temperature lapse rate for a lifting air mass cools at dry conditions is -0.0098 ºC m^{-1} (dry adiabatic lapse rate) and about -0.0065 ºC m^{-1} under saturated conditions (saturated adiabatic lapse rate). The adiabatic lapse rates are governed by pressure changes in the atmosphere. The environmental lapse rate (ELR), which is the change of temperature with elevation in the free atmosphere, averages about -0.0065 ºC m^{-1}, but can exhibit variation in different layers (Rolland, 2003). Conversely, in the near-surface layer the NSTGE are influenced by factors as the local energy balance regime, topography, moisture, synoptic conditions, microclimate, etc., so that the NSTGE normally are different to the free-air temperature lapse rate (Blandford et al., 2008).

While temperature usually decreases with increases in elevation (negative NSTGE), the atmosphere can be isothermal or the NSTGE can be positive, i.e., temperature can increase with increases in elevation (Navarro-Serrano et al., 2018). These patterns can be due to the cold air drainage phenomenon, which occurs (normally at night) when there is relatively high atmospheric pressure and little wind, under stable atmospheric conditions (Gustavsson et al., 1998). The cold air accumulates in lower elevation areas (like ditches or valleys) resulting in a temperature inversion (Hubbart et al., 2007). When cold air drainage occurs, NSTGE can reach very high values. A few examples follow: Foster et al. (2017) found a difference of temperature of 15 ºC between 1800 and 2500 m a.s.l. (around +0.021 ºC m^{-1}) in Salt Lake Valley, Utah;

Gerlitz et al. (2016) obtained up to +0.03 ^{o}C m^{-1} for a slope of the Rolwaling Himal in Nepal; Hubbart et al. (2007) found inverted NSTGE that differ from the expected lapse rates by more than +0.08 ^{o}C m^{-1} for the Mica Creek Experimental Watershed located in northern Idaho; Grudzielanek and Cermak (2018) obtained values higher than +1.3 ^{o}C m^{-1} using thermal infrared imaging at the northern fringe of the Rhenish Massif in Bochum, Germany. In contrast, inversions in NSTGE during the daytime are usually caused by a greater heating of the high elevation areas of the mountains due to higher solar radiation (Kattel et al., 2015). Depending on the scale, the actual pattern in NSTGE may be difficult to estimate, which may produce errors that will be propagated through the estimates used in models (Lookingbill and Urban, 2003).

The objectives of this work are (1) to compare the MODIS-based land surface temperature (LST) to near-surface meteorological data at two different scales, (2) to assess the variability of temperature by identifying the correlation with elevation at both scales, and (3) to identify local factors that influence the correlation of near-surface temperature with elevation and justify different rates at the two scales. Note that the study area and the ranges of elevation for the two scales explored are different. The coarse scale across the northern Front Range of Colorado (NFRC) used data from the Natural Resources Conservation Service (NRCS) automated Snowpack Telemetry (SNOTEL) network ranging in elevation from 2612 and 3265 m a.s.l. over an area of about 4800 km². At the fine scale over a 0.4 km² area, iButton sensors were installed with an elevation range from 2745 to 2804 m a.s.l at the Colorado State University Mountain Campus (CSU-MC) located within the NFRC. The coarse-scale NRFC LST-

SNOTEL evaluation is an area to point comparison, while the fine-scale CSU-MC LST-iButton evaluation is an area to area comparison. While many research studies apply interpolation techniques to combine LST and temperature observation data (Bosilovich, 2006; Stewart and Nitschke, 2017), this paper does not focus on such methods.

2. Case study and data

2.1 Location and climate

The NFRC study area is located within the Southern Rocky Mountains and includes Rocky Mountain National Park (Figure 1) with Longs Peak at the highest elevation of 4346 m a.s.l. The CSU-MC is located in the Pingree Park Valley below the Mummy Range at an approximate elevation of 2745 m. CSU-MC covers an area of about 6.5 km^2 of the South Fork of the Cache la Poudre River (SFCLR) basin (Figure 1). The NFRC is a semi-arid region that is cool at night and warm during the day in spring, summer and fall, and cold in the winter (Goble, 2017). Total annual precipitation varies from 500 to 1100 mm at the SNOTEL stations, with only 120 to 300 mm coming when there is no snow cover (Fassnacht, in review). Snow is intermittent below about 2000 meters; across the study SNOTEL stations and the CSU-MC snow is persistent through the winter season (Kampf and Fassnacht, 2020).

2.2 Temperature datasets

2.2.1 SNOTEL stations

The SNOTEL network was established to measure the snowpack and to forecast streamflow originating as snowmelt in the mountains of the Western United States

(Natural Resources Conservation Service, 2019). The stations are powered by solar panels and measure the snowpack (snow water equivalent or SWE, and depth), precipitation, temperature, and other climatic variables (at some stations); hourly data are available in real-time through meteor burst telemetry (Natural Resources Conservation Service, 2016). Data from the SNOTEL network have been used for hydrological and climatological studies (e.g. Wrzesien et al., 2015; Fassnacht et al., 2017).

We used hourly temperature data collected over a 35-day period between August 25 and September 28, 2018 from 21 SNOTEL stations across the NFRC (Figure 1) at a density of one station per 230 km^2 (or one every 15 km). These data are available from the NRCS at <wcc.nrcs.usda.gov> (Natural Resources Conservation Service, 2016). The selected SNOTEL stations ranged in elevation from 2612 to 3265 m. The SNOTEL stations use YSI extended range temperature sensors <ysi.com/> that are housed within a radiation shield. Each temperature sensor is located approximately 4 meters above the ground on a cross-arm mounted on a triangular tower opposite the SNOTEL snow pillow that measures SWE.

2.2.2 Temperature sensors

In the last few decades, alternatives to the traditional meteorological stations have entered the market. Individual temperature sensors with a relatively low-cost are now available (e.g. Hobo, Stowaway Tidbit Thermochron iButton, Blue Maestro). The Hobo sensor (Whiteman et al., 2000) and Thermochron iButton sensor (Hubbart et al., 2005) have been evaluated and found to have satisfactory accuracy compared to more

expensive traditional sensors. The small size (now 1-2 cm in diameter and 0.5 cm thick) and low price are the main advantage compared to automatic stations, but solar radiation shields (e.g. Gill radiation shields by R.M. Young Co., or Spectrum radiation shields by Spectrum Technologies) have a high cost, which can limit the optimal use of these newer sensors. However, costs can be reduced by using alternative radiation shields, such as a double funnel system (Hubbart, 2011), using evergreen trees as a radiation shield (Lundquist and Huggett, 2008), or a combination of the two methods.

For the fine-scale analysis at the CSU-MC, 12 temperature-only and five temperature-humidity sensors were deployed (Figure 1) for the same 35-day period. The mean horizontal distance between stations was 48 meters. The temperature sensors collected data every 10 minutes, and the temperature-humidity sensors every 20 minutes. These were averaged to the same hourly time step as the SNOTEL data (Fassnacht et al., 2019). The temperature sensors were Thermochron iButton devices from <maximintegrated.com> that measured temperature in 1/8°C increments with a stated accuracy of ±1°C. The temperature-humidity sensors were Hygrochron Temperature/Humidity Logger iButton devices from <maximintegrated.com> that measured humidity with 12-Bit (0.04%RH) resolution (accuracy unstated by manufacturer), and temperature with 11-Bit (0.0625°C) resolution with a stated accuracy better than ±0.5°C.

The sensors were housed within a double-set of ordinary white kitchen funnels serving as a radiation shield. The 15.2 cm tall outside funnel was 14 cm in diameter, and the 12.7 cm tall inside funnel was 12 cm in diameter with about 12 holes of 0.64 cm

diameter drilled into it for air flow, as per Hubbart (2011). Each shielded sensor was placed approximately 2-m above the ground on the north side of an evergreen tree to shelter it from overheating by radiative exchange when measuring air temperature (Lundquist and Huggett, 2008). We calibrated the sensors by storing them in close proximity to one another for several hours before and after deployment. The differences between sensor measurements were typically 0.5 °C with a maximum difference of 1.0 °C occurring for less than 5% of all calibration measurements. All data were visually inspected to assess obvious outliers; only measurements taken while the sensor was being downloaded were eliminated (<0.1% of all the data).

2.2.3 Remotely sensed LST

The remotely sensed MODIS LST and Emissivity (MOD11A1) product available from the NASA Distributed Active Archive Center (DAAC) <*earthdata.nasa.gov*> has a spatial resolution of about 1 km using a sinusoidal projection and provides daily daytime and nighttime data. We used the same 35-day period as for the SNOTEL station and iButton sensor analysis. Note that the product MOD11A1 can have some gaps due to presence of clouds in images, the presence of dust in the atmosphere, and sensor failure. Three MODIS tiles covering NFRC (h09v04, h09v05 and h10v04) were extracted. From these tiles six grids around the CSU-MC (Figure S1) and 21 grids corresponding to the SNOTEL stations were selected (Figure 1).

2.3 Elevation Dataset

The elevation data were obtained from the National Elevation Dataset digital elevation model of the United States Geological Survey available at <*nationalmap.gov*>. The spatial resolution is 1/3 arc-second (about 10 meters). The elevation of each iButton sensor, SNOTEL station, and across each MODIS LST grid (e.g., Figure S1) were extracted from the National Elevation Dataset digital elevation model.

3. Methodology

To assess the spatial accuracy of remote sensing LST at coarse and fine scales (represented by the SNOTEL stations and iButton sensors respectively), we (1) compared the mean of the MODIS LST data and the individual temperature (SNOTEL and iButton) measurements considering only the information that correspond to the view time (instantaneous observations) of the LST product in the studied period, and (2) analyzed the spatiotemporal relation of temperature versus elevation for the three data sources. We used the same temporal reference, specifically GMT-7, for all hourly data and downloaded the time views of the MODIS LST product for the daytime and nighttime observations. SNOTEL and iButton data have a point-support while satellite derived temperatures have an area-support whose resolution is the size of the image pixels. When data with different spatial supports are compared or integrated to produce a new product, geostatistical approaches should be applied to combine them (Kyriakidis, 2004; Comber and Zeng, 2019). However, in some hydrological studies temperature point data are used to represent a certain area (Martinec et al., 1998). In this

study we aim to highlight the possible implications of using either source of information and the spatial support is not considered.

The mean and standard deviation were computed per daytime and nighttime acquisition of LST compared to the SNOTEL (coarse) and iButton (fine) scale station and sensor data. All individual measurements were also compared and the Nash-Sutcliffe efficiency (NSE) coefficient were calculated for those. The coarse-scale evaluation of MODIS LST versus SNOTEL stations was considered an area (pixel) to point (one station per pixel) comparison, while the fine-scale evaluation of MODIS LST versus the iButton sensors was considered an area (pixel) to area (multiple sensors per pixel) comparison.

We analyzed the temperature and elevation correlation by using a linear regression model:

$$T = Sz + c \quad (1)$$

where T represents the temperature (ºC), z the elevation (m), and S (ºC m^{-1}) and c (ºC) are best-fit parameters to be estimated for each hour from the iButton sensors or SNOTEL stations. In the case of MODIS LST, the linear regression models were defined for each view time of the satellite (Figure 3). The coefficient of determination (R^2) and the slope or gradient (parameter S) of the hourly models were obtained and used to obtain the hourly elevation patterns of temperature at the two spatial scales considered. R^2 indicates the degree of correlation between temperature and elevation. The slope shows the NSTGE and its possible inversions when positive values (increment of temperature with elevation) are obtained. The slope and R^2 of the linear

correlation between elevation and temperature allowed us to evaluate the elevation patterns at the two scales studied. Mean NSTGE have been calculated in two different ways: (1) by using the relationship between mean temperature per location and elevation, and (2) as the mean of the hourly NSTGE. The second procedure allowed considering outliers by using different thresholds of R^2 associated to each hourly NSTGE.

4. Results

The MODIS LSTs are on average warmer than SNOTEL stations during the day (Figure 2a and 2e) and the iButton sensors at night (Figure 2d). Conversely, the average nighttime SNOTEL temperatures are warmer than the MODIS LST (Figure 2b and 2f), while the daytime MODIS LST are most similar to the average iButton temperatures (Figures 2c and S2a). The NSE coefficient of the MODIS LST and the measured temperature is below zero for the coarse scale and the nighttime of the fine scale. MODIS LST shows higher accuracy at the finer scale in the daytime (NSE 0.42). The values of the linear correlation (y-intercept and slope) between MODIS LST and SNOTEL (area to point comparison) temperature for each day show a linear correlation between them too (Figure S3), being more correlated in the daytime than nighttime (0.92 vs 0.76). Therefore, the biases between the two sources of information could be defined by one independent value assuming those correlations are reasonable. For SNOTEL station and nighttime iButton comparisons, the MODIS LSTs are generally warmer at cooler temperatures and cooler at warmer temperatures as illustrated by the

slopes in the range of 0.5 (Figures 2a, 2b, and 2d). On average the daytime MODIS LSTs are about 1ºC cooler than the iButton temperatures (Figure 2c and S2a).

Day view times for the MODIS LST are between 10:00 and 12:00 with night view times between 21:00 and 23:00, which are a few hours after sunrise and sunset, respectively (Figure 3). The daytime correlation between temperature and elevation is much better for the SNOTEL stations with R^2 mostly between 0.3 and 0.8 than MODIS LST with R^2 between 0 and 0.4 (Figure 3a top-right plot). The temperature-elevation correlation for night increases for MODIS LST and decreases for SNOTEL (Figure 3a top-left plot). At the finer scale (showed in Figure 3b top plots), MODIS LST and iButtons show similar correlation between temperature and elevation (an average of 0.36 and 0.32 respectively) while during the nighttime the correlations are higher for the iButtons (0.54 vs 0.24). NSTGE are more consistent between MODIS LST and the measured temperature at SNOTEL stations for the coarse scale. Both sources of data show negative NSTGE being more similar during the nighttime (Figure 3a bottom plots). However, the NSTGE for the MODIS LST data are very different compared to the iButton data (see Figure 3b bottom plots) and even during the daytime the NSTGE are opposite, i.e., iButton shows positive values and MODIS LST negative values.

In Figure 4, the characterization of the NSTGE with elevation at the two resolutions is examined as an average of the study period; Figure 3 shows daily NSTGE. For the SNOTEL resolution (Fig. 4a), both daytime and nighttime temperatures follow the theoretical ELR, with decreasing temperature with elevation of 0.0068 ºC m^{-1} and 0.0049 ºC m^{-1}, respectively. While daytime temperature shows a

good agreement with elevation across the study area ($R^2 = 0.74$), nighttime temperature correlation with elevation is less evident ($R^2 = 0.19$), indicating the possible influence of local phenomena during the cooling hours, such as thermal inversion occasionally noted at some of the SNOTEL locations. Conversely, at the valley resolution with iButton records (Fig. 4a), we observe a totally inverted NSTGE (increasing temperatures with elevation), especially during the nighttime (0.0975 $^{o}C\ m^{-1}$), but in both cases, daytime and nighttime are significant. Both positive NSTGE indicate persistent thermal inversion conditions that can be explained by different local mechanisms such as differential insolation and katabatic winds, as we will later discuss.

The capacity of the MODIS LST products to replicate NSTGE with elevation is fair at the SNOTEL resolution (Fig. 4b); decreasing temperature is estimated with elevation for both daytime and nighttime, although, contrary to SNOTEL observations, for MODIS the correlation of temperature with elevation (and the NSTGE) is higher at nighttime, and weaker in daytime. At the valley resolution, MODIS shows no capability for reproducing observed NSTGE (Fig.4b). In the daytime it produces a negative NSTGE, while observations show a positive NSTGE. In the nighttime it estimates a positive and weak (low R^2) NSTGE compared to observations.

The NSTGE presented in Figure 4 were calculated using the mean land surface temperature over the 35-day study period. Alternatively, mean NSTGE have been calculated as the average of the hourly values (first row of Table 1), which present slight differences with those shown in Figure 4. We have also calculated mean NSTGE considering the values which have associated R^2 values above different thresholds (0.1,

0.2, 0.3, and 0.4) (see Table 1). Thus, we are considering the hourly NSTGE as outliers, which have associated a value of R^2 lower than a specific threshold. In general the absolute value of the hourly NSTGE increases with R^2 (see Figure S4). If the NSTGE with associated values of R^2 lower than 0.2 are considered outliers, the absolute increment of them with respect not considering this threshold are 15 and 38% for SNOTEL stations, 46 and 25% for iButton sensors, 87 and 9% for MODIS pixels at SNOTEL locations, and 18 and 62% for MODIS pixels at iButton locations for daytime and nighttime respectively.

The differing behavior of temperatures with elevation between day and nighttime is further confirmed if we examine the evolution of coefficients (correlation and NSTGE) each hour throughout the day (Figure 5). At the SNOTEL scale, the correlation between temperature and elevation are negative over the entire day (temperature decreases with elevation) and the higher negative correlations (R close to -0.9) are observed during the daytime (10h to 18h) (Figure 5a). Conversely, at the iButton scale, the correlation between temperature and elevation are almost always positive over the entire day (temperature increases with elevation) and we observe (Figure 5c) higher positive correlations (R close to 0.8) during the nighttime (20h to 6h). The NSTGE follow the same hourly pattern (Fig. 5b and 5d), and interestingly, they are in phase with the spatial variability of temperature (standard deviation amongst locations) during the day. At both scales, the standard deviation of temperature is low during the daytime hours, and rises towards the nighttime, confirming that local factors affecting the NSTGE similarly affect the spatial variability of temperature. This is

especially true during the night. Moreover, this effect is larger at the fine scale, confirming the role of topographic factors for conditioning spatial variability of temperature at the local scale (Figure 5d).

The NSTGE and the strength of the temperature-elevation correlation vary by day and time of day (Figure 6). At the coarse scale, the correlation is typically strongest in the afternoon (average R^2 values of 0.7 in Figure 6a) with a NSTGE of about -0.0075 $^oC\ m^{-1}$ (Figure 6c). The correlation becomes weak at night (average R^2 of 0.2) and is weakest in early morning (Figure 6a). The nighttime NSTGE decreases from -0.005 to -0.003 $^oC\ m^{-1}$ as the night progresses (Figure 6c).

Air temperatures cool less than 5^{o}C from 18:00 to 23:00 for six of the 35 nights (Figures 6e and 6f). When there is less cooling, the temperature-elevation correlation is strong at night over the coarse scale (Figure 6a). More noticeably, the correlation at the fine scale is poor for those six days where nightly cooling is limited (Figure 6b). The observed usual thermal inversion disappears during those six days when warmer nighttime conditions occur. This reinforces the idea that the persistent inversion of the NSTGE at the valley scale is due to local night winds (katabatic cool drainage) that may become weaker depending on the meteorological conditions (e.g. cloudiness, instability). Different wind conditions exist for daytime and nighttime (see Figure S5; Note that wind speed and direction data were only available from September 11 through 28). Generally, the wind speeds and the R^2 of the SNOTEL data (versus elevation) are higher during the daytime, and the nights with higher R^2 for the iButton data occurred when wind speeds were low (Figure S5a). Similarly, higher R^2 values for the iButton

data during nighttime are observed when there is less cooling and the wind speed is low (Figure S5b). During the daytime the wind direction is more variable than at the nighttime, with the wind direction showing a clear difference between the cooling nights (prevalent direction of 200°) and limited cooling nights (prevalent direction of 230°) (Figure S5c). As stated earlier, for these limited cooling nights the temperature-elevation correlation is strong for the coarse scale and poor for the fine scale when a thermal inversion establish.

In the absence of data, we typically assume the theoretical ELR to interpolate. At the coarse scale this is reasonable (Figure S6a) across a watershed (Figure 1a). However, at the fine scale, the errors can be large (Figure S6b) if we use the theoretical ELR for interpolating across a smaller area, such as a lateral moraine (Figure 1b).

5. Discussion

There are several LST products available with different spatial resolution, orbital frequency, and temporal coverage. Some products have spatial resolutions finer than 100 m (e.g., LANDSAT or ASTER) but with a low temporal resolution (around 16 days for the first example and between 4 and 16 days for the second) to characterize some hydrological processes. The MODIS LST product has a twice-daily temporal resolution and has thus been used in hydrologic studies (Wang et al., 2009; Khorchani et al, 2018). In this work, we have encountered important biases between measured temperature and LST of the MODIS product for the two scales studied: (1) area to point (using SNOTEL measurements) and (2) area to area (using iButton measurements). These biases in mean

temperature and NSTGE are not consistent for the different scales (Figures 2 and 3). The different spatial supports can partially explain the differences detected between MODIS LST and temperature observations and the integrated analyses of them could be analyzed in a future research. Other authors also illustrated discrepancies in satellite LST products compared to ground measurements, so that retrieving LST from space-based thermal infrared data is still a challenge (Li et al., 2013; Li and Duan, 2018). However, in other applications, these LST products have been used as secondary information to estimate air temperature obtaining satisfactory results (Kloog et al., 2014; Yang et al., 2017). In view of the results, each case study should be examined when LST products are used in favor of measured data from sensors or stations. In general, the support (Blöschl, 1999) of the MODIS LST is an aerial average over 1-km, while the support of the SNOTEL station is essentially a point, especially due to local variability (Ma et al., 2019).

The characterization of temperature patterns with elevation for the two scales investigated here have been done using two sources of information, SNOTEL and iButton data. While the accuracy of the iButton assessments was found to be satisfactory (Hubbart et al., 2015), some authors have identified problems in terms of accuracy and uniformity for temperature from SNOTEL measurements (Chelliah and Ropelewski, 2000; Julander et al., 2007). These issues are currently being evaluated (Oyler et al., 2015; Fassnacht et al., 2017; Ma, 2017; Ma et al., 2019). Further, the SNOTEL temperature sensors are at a height of 4 m above the ground, while the iButton sensors were installed at 2 m above the ground. The nighttime iButton

temperatures are similar to the SNOTEL temperatures at a similar elevation (Figure 4a), such as the Phantom Valley station that is at 2753 m.a.s.l. (seen below the iButton nighttime best fit line in Figure 4a). The Hourglass Lake station is higher than the iButton transect at 2860 m.a.s.l., but it is the closest SNOTEL station to CSU-MC. Daytime temperature was on average warmer for the iButton sensors than the SNOTEL stations of similar elevation (Figure 4a).

We observe important differences between the temperature patterns of the two scales studied. These differences can be explained by local conditions that can modify the temperature patterns (Dobrowski et al., 2009; Martin et al., 2019) and can be influenced by the different elevation ranges where the stations or sensors are located. For example, the inversion of the NSTGE detected from the iButton measurements that intensified during the nighttime in the Pingree Valley, can be explained by cold air drainage. This phenomenon usually occurs at night, due to katabatic winds (downslope winds flowing from high elevations of mountains) induced by the higher density of cold air at higher elevations once there is no insolation (Clements et al., 2003). This pattern has been encountered in other case studies (Bergen, 1969; Hubbart et al., 2007; Bigg et al., 2014; Gertlitz et al., 2016; Foster et al., 2017; Grudzielanek and Cermak, 2018). However, we also observed an inverse NSTGE during daytime in the Pingree Valley. Reductions or inversions in NSTGE during the daytime are usually caused by greater heating of the higher elevations due to greater amounts of solar radiation (differential insolation) (Kattel et al., 2015). Both phenomena are very dependent on weather conditions (Barr and Orgill, 1989; Pepin et al., 2011).

The NSTGE in the valley are much greater than those at the coarse scale. While NSTGE obtained for the coarse scale are around the theoretical ELR, in the valley we calculated average 0.034 and 0.0975 ºC m^{-1} NSTGE for the daytime and nighttime, respectively. These values are almost an order of magnitude greater than the dry and saturated adiabatic lapse rates (-0.0098 and -0.0065 ºC m^{-1}) due to the cold air drainage affecting the valley. In previous studies values similar to our daytime (Foster et al., 2017; Gertliz et al., 2016) and nighttime (Hubbart et al., 2007) NSTGE were found, as well as larger NSTGE values (Grudzielanek and Cermak, 2018).

The NSTGE can be very different to free air temperature lapse rates. The former can be affected by micro-scale factors such as cold air drainage, cast shading or differential insolation between slopes (Hubbart et al., 2007; Zhang et al., 2018). This finding points to the very high variability of the temperature conditioning factors (mainly cold air drainage and differential insolation) in the Pingree Valley (Figure 1b).

In this study, MODIS LST shows a higher accuracy at the fine scale and during the daytime period (Figure 2c), when the phenomenon of cold air drainage is not acting, but this accuracy is not sufficient for hydrological applications. Therefore, LST from satellite data should be used with caution. The information should be verified with secondary data from stations or sensors because coarse-scale satellite data can introduce errors in the characterization of the temperature patterns that can then be propagated to hydrological or agricultural models (Hulley et al., 2012; Ghent et al., 2019). Sometimes when temperature data are limited, satellite data are extrapolated between different scales, usually using geostatistical estimations including secondary information as

elevation or NSTGE (Monestiez et al., 2001; Naseer et al., 2019). However, as shown in this study, temperature patterns between scales can vary considerably and a proper characterization of the patterns of temperature variability at differing elevations is needed. Otherwise uncertainties will be propagated to the estimations used for modeling. In the case study, from the point of view of the interpolation considering NSTGE, the theoretical ELR could be representative of the coarse scale (SFCLR watershed) but not of the fine scale (lateral moraine) (Figure S6).

The data used in this study were obtained for a short temporal period (35 days) when data at both scales were available (Fassnacht et al., 2019). Future work should explore a longer study period, which could contribute more insight into the cold air drainage and other local phenomena. Similarly, further investigations across medium scales, such as at the watershed scale (dendritic features in Figure 1a), could identify the scale of cold air drainage patterns. Such two future examinations could capitalize (Fassnacht et al., 2014) on the regional density of SNOTEL stations in mountain region data by installing additional inexpensive, stand-alone temperature sensors, such as those used here.

6. Conclusions

In this research study we compared measured temperatures at two different scale resolutions with remote sensing LST data in terms of mean, standard deviation, correlation coefficient (R^2), and slope of the linear regression between temperature and elevation. MODIS LST overestimates nighttime temperatures at fine scales and daytime

temperatures at coarse scales, while MODIS LST underestimates daytime temperatures at fine scales and nighttime temperatures at coarse scales. MODIS LST does not show an inverse NSTGE at the fine scale (as observed in the Pingree Valley during the daytime and nighttime) and the NSTGE in absolute value is much lower than that of the iButton sensors. In view of the results, a proper evaluation of LST products is necessary before using them in finer-scale hydrological or agricultural assessments since the uncertainties in temperature relations can be propagated to the final results.

We also assessed the variability of temperature at two spatial scales through the study of the NSTGE. Despite both case studies' locations in the same mountain region (the fine scale case is located within the coarse scale case), we observed different patterns of temperature. The R^2 value for the linear correlation between temperature and elevation is higher during the nighttime, showing an inverse NSTGE in the case of the fine scale data. However, R^2 is higher during the daytime, and the temperature decreases with elevation at the coarse scale. With respect to the NSTGE, the daytime and nighttime temperature follows the theoretical ELR at the coarse scale of the SNOTEL stations. However, inverse and extreme NSTGE are observed at the finer scale (Pingree Valley). They are due to the phenomena of cold air drainage acting during the nighttime and differential insolation during the daytime. Therefore, when elevation is used as secondary information to supplement temperature data, caution should be used extrapolating those patterns between different scales. Micro-scale climatology in mountain regions can contradict physical assumptions normally made for larger scales. Phenomena, such as cold air drainage, can modify the local distributions of temperature

with elevation. This work reveals the necessity of micro-scale analyses for validation of climatic products in mountain areas.

Acknowledgements

We thank the Spanish Ministry of Science, Innovation and Universities for the funds provided through the program of pre-doctoral mobility (reference EEBB-I-2018-12762) and the research project SIGLO-AN (RTI2018-101397-B-I00), which has helped to perform this collaborative work during and after the stay of Collados-Lara at Colorado State University. We also thank the Colorado State University Warner College of Natural Resources Mountain Campus Research Support Fund (created by Dr. James R. Meiman) for the support to install the temperature sensors.

Datasets

The SNOTEL temperature data were obtained from the Natural Resources Conservation Service <wcc.nrcs.usda.gov>. The MODIS land surface temperature data (product MOD11A1) were retrieved from the NASA Distributed Active Archive Center (DAAC) <earthdata.nasa.gov>. The digital elevation model was retrieved from the United States Geological Survey National Elevation Dataset <*nationalmap.gov*>. The iButton data are available at <doi.pangaea.de/10.1594/PANGAEA.907034> (Fassnacht et al., 2019).

Supporting information

Figure S1. Hypsometric curves (distribution of elevation) for the six MODIS LST grids in an around the iButtton sensors, as per Figure 1.

Figure S2. Mean and standard deviation of temperature of the iButton data and MODIS LST for the grids within the CSU-MC for the a) daytime and b) nighttime view time of the Aqua-Terra satellites. Note that in (b) are not represented 35 points because the product MOD11A1 has some gaps.

Figure S3. Best fit linear slope versus y-intercept for the MODIS-SNOTEL temperature data from each day with daytime and nighttime separated. The goodness of fit per day is shown by the bubble size.

Figure S4. NSTGE versus coefficient of determination (R^2) of the hourly linear relationship between temperature and elevation for a) SNOTEL stations, b) iButton network, c) MODIS estimates for SNOTEL pixels, and d) MODIS estimates for iButton pixels, for the daytime and nighttime periods.

Figure S5. Coefficient of determination (R^2) between SNOTEL versus iButton showing for a) daytime (in orange) and nighttime periods (in grey), and b) cooling (in purple) and low cooling nights (green). The cooling nights are based on a decrease of at least 5^{o}C from 18:00 to 23:00. The bubble size indicates the hourly wind speed. Note that the wind speed and direction data were only available from September 11th through 28th**.**

Figure S6. Mean temperature obtained by using a theoretical ELR of -0.0065 ^{o}C m-1 versus using the daily obtained NSTGE for a) the SFCLR watershed (coarse scale) and b) the lateral moraine (fine scale). Both include fit lines and the RMSE and NSE statistics for data with $R^2 \geq 0.2$ and $R^2 < 0.2$.

References

Barr, S. & Orgill, M. M. (1989). Influence of External Meteorology on Nocturnal Valley Drainage Winds. Journal of Applied Meteorology, 28, 497–517, https://doi.org/10.1175/1520-0450(1989)028<0497:IOEMON>2.0.CO;2

Bayat, B., Zahraie, B., Taghavi, F., & Nasseri, M. (2013). Evaluation of spatial and spatiotemporal estimation methods in simulation of precipitation variability patterns.

Theoretical and Applied Climatology, 113(3-4), 429–444. https://doi.org/10.1007/s00704-012-0795-7

Benavides, R., Montes, F., Rubio, A., & Osoro, K. (2007). Geostatistical modelling of air temperature in a mountainous region of Northern Spain. Agricultural and Forest Meteorology, 146(3-4), 173–188. https://doi.org/10.1016/j.agrformet.2007.05.014

Bergen, J. D. (1969). Cold Air Drainage on a Forested Mountain Slope. Journal of Applied Meteorology, 8, 884–895. https://doi.org/10.1175/1520-0450(1969)008<0884:CADOAF>2.0.CO;2

Bigg, G. R., Wise, S. M., Hanna, E., Mansell, D., Bryant, R. G., & Howard, A. (2014). Synoptic climatology of cold air drainage in the Derwent Valley, Peak District, UK. Meteorological Applications, 21, 161–170. https://doi.org/10.1002/met.1317

Blandford, T. R., Humes, K. S., Harshburger, B. J., Moore, B. C., Walden, V. P. & Ye, H. (2008). Seasonal and Synoptic Variations in Near-Surface Air Temperature Lapse Rates in a Mountainous Basin. J. Appl. Meteor. Climatol., 47, 249–261. https://doi.org/10.1175/2007JAMC1565.1

Blöschl, G., (1999). Scaling issues in Snow Hydrology. Hydrological Processes, 13(14-15), 2149 -2175. https://doi.org/10.1002/(SICI)1099-1085(199910)13:14/15<2149::AID-HYP847>3.0.CO;2-8

Bosilovich, M. G. (2006). A comparison of MODIS land surface temperature with in situ observations. Geophys. Res. Lett., 33, L20112. https://doi.org/10.1029/2006GL027519.

Chelliah, M., & Ropelewski, C. F. (2000). Reanalysis-based tropospheric temperature estimates: Uncertainties in the context of global climate change detection. Journal of Climate, 13, 3187–3205. https://doi.org/10.1175/1520-0442(2000)013<3187:RBTTEU>2.0.CO;2

Chen, F., Yang, X., Ji, C., Li, Y., Deng, F., & Dong, M. (2019). Establishment and Assessment of Hourly High-resolution Gridded Air Temperature Datasets in Zhejiang, China. Meteorological Applications, 26(3), 396–408. https://doi.org/10.1002/met.1770

Clements, C. B., Whiteman, C. D., Horel, J. D. (2003). Cold-air-pool structure and evolution in a mountain basin: Peter Sinks, Utah. Journal of Applied Meteorology, 42, 751–768. https://doi.org/10.1175/1520-0450(2003)042<0752:CSAEIA>2.0.CO;2

Collados-Lara, A. J., Pardo-Igúzquiza, E., & Pulido-Velazquez, D. (2018). Precipitation fields in an alpine Mediterranean catchment: Inversion of precipitation gradient with elevation or undercatch of snowfall?. International Journal of Climatology, 38, 3565–3578. https://doi.org/10.1002/joc.5517

Collados-Lara, A. J., Pardo-Igúzquiza, E., & Pulido-Velazquez, D. (2019). A distributed cellular automata model to simulate potential future impacts of climate change on snow cover area. Advances in Water Resources, 124, 106–119. https://doi.org/10.1016/j.advwatres.2018.12.010

Comber, A., Zeng, W. (2019) Spatial interpolation using areal features: A review of methods and opportunities using new forms of data with coded illustrations. Geography Compass, 13, e12465. https://doi.org/10.1111/gec3.12465

Dobrowski, S. Z., Abatzoglou J. T., Greenberg J. A., & Schladow S. G. (2009). How much influence does landscape-scale physiography have on air temperature in a mountain environment?. Agricultural and Forest Meteorology, 149(10), 1751–1758. https://doi.org/10.1016/j.agrformet.2009.06.006

Fassnacht, S. R., Allegretti, A. M., Venable, N. B. H., Fernández-Giménez, M. E., Tumenjargal, S., Kappas, M., Laituri, M. J., Batbuyan, B., & Pfohl, A. K. D. (2018). Merging Indigenous Knowledge Systems and Station Observations to Estimate Uncertainty of Precipitation Change in Central Mongolia. Hydrology, 5(3), 46. https://doi.org/10.3390/hydrology5030046

Fassnacht, S.R, Collados-Lara, A.-J., Pfohl, A.K.D., Venable, N.B.H., & Puntenney-Desmond, K. (2019). Fine Spatio-temporal Resolution Temperature and Humidity iButton Data at the Colorado State University Mountain Campus, August 25 to September 28, 2018. PANGAEA. https://doi.pangaea.de/10.1594/PANGAEA.907034

Fassnacht, S. R., Deitemeyer, D. C., & Venable, N. B. H. (2014). Capitalizing on the daily time step of snow telemetry data to model the snowmelt components of the hydrograph for small watersheds. Hydrological Processes, 28(16), 4654-4668. https://doi.org/10.1002/hyp.10260

Fassnacht, S. R., López-Moreno, J. I., Ma, C., Weber, A. N., Pfohl, A. K. D., Kampf, S. K., & Kappas, M. (2017). Spatio-temporal Snowmelt Variability across the Headwaters of the Southern Rocky Mountains. Frontiers of Earth Science, 11, 505–514. https://doi.org/10.1007/s11707-017-0641-4.

Fassnacht, S. R., Patterson, G. G., Venable, N. B. H., Cherry, M. L., Pfohl, A. K. D., Sanow, J.E., & Tedesche, M.E. (in review). How Do We Define Climate Change? Considering the Temporal Resolution of Niveo-meteorological Data. Hydrology (submitted 29 June 2020, hydrology-747330R1).

Foster, C.S., Crosman, E.T. & Horel, J.D. 2017. Simulations of a Cold-Air Pool in Utah's Salt Lake Valley: Sensitivity to Land Use and Snow Cover. Boundary-Layer Meteorol 164, 63–87 (2017). doi: 10.1007/s10546-017-0240-7

Gerlitz, L., Bechtel, B., Böhner, J., Bobrowski, B., Bürzle, B., Müller, M., Scholten, T., Schickhoff, U., Schwab, N., Weidinger, J. 2016. Analytic comparison of temperature lapse rates and precipitation gradients in a Himalayan treeline environment – Implications for statistical downscaling. In: Singh RB, Schickhoff U, Mal S (eds) Climate change, glacier response, and vegetation dynamics in the Himalaya. Springer, Cham, pp 49–64. doi: 10.1007/978-3-319-28977-9_3

Ghent, D., Veal, K., Trent, T., Dodd, E., Sembhi, H., & Remedios, J. (2019). A New Approach to Defining Uncertainties for MODIS Land Surface Temperature. Remote Sensing, 11(9), 1021. https://doi.org/10.3390/rs11091021

Goble, P. (2017). "Colorado Climate," Colorado Encyclopedia, last modified October 07, 2019, https://coloradoencyclopedia.org/article/colorado-climate.

Grudzielanek, A.M., Cermak, J. 2018. Temporal Patterns and Vertical Temperature Gradients in Micro-Scale Drainage Flow Observed Using Thermal Imaging. Atmosphere, 9, 498. doi: 10.3390/atmos9120498.

Gustavsson, T., Karlsson, M., Bogren, J., &Lindqvist, S. (1998): Development of Temperature Patterns during Clear Nights. J. Appl. Meteor., 37, 559–571, https://doi.org/10.1175/1520-0450(1998)037<0559:DOTPDC>2.0.CO;2

Hannah, D. M., Demuth, S., van Lanen, H. A. J., Looser, U., Prudhomme, C., Rees, G., Stahl, K., & Tallaksen, L. M. (2011). Large-scale river flow archives: Importance, current status and future needs. Hydrological Processes, 25(7), 1191–1200. https://doi.org/10.1002/h yp.7794

Hubbart, J. (2011). An Inexpensive Alternative Solar Radiation Shield for Ambient Air Temperature Micro-Sensors. Journal of Natural & Environmental Sciences, 2 (2), 9–14.

Hubbart, J., Kavanagh, K. L., Pangle, R., Link, T., & Schotzko, A. (2007). Cold air drainage and modeled nocturnal leaf water potential in complex forested terrain. Tree Physiology, 27, 631–639. https://doi.org/10.1093/treephys/27.4.631

Hubbart, J., Link, T., Campbell, C., & Cobos, D. (2005). Evaluation of a low-cost temperature measurement system for environmental applications. Hydrological Processes, 19, 1517–1523. https://doi.org/10.1002/hyp.5861

Hudson, G., & Wackernagel, H. (1994). Mapping temperature using kriging with external drift: theory and an example from Scotland. International Journal of Climatology, 14(1), 77–91. https://doi.org/10.1002/joc.3370140107

Hulley, G. C., Hughes, C. G., & Hook, S. J. (2012). Quantifying uncertainties in land surface temperature and emissivity retrievals from ASTER and MODIS thermal

infrared data. Journal of Geophysical Research, 117, D23113. https://doi.org/10.1029/2012JD018506

Irvine, D. J., Briggs, M. A., Lautz, L. K., Gordon, R. P., McKenzie, J. M., & Cartwright, I. (2017). Using Diurnal Temperature Signals to Infer Vertical Groundwater-Surface Water Exchange. Groundwater, 55, 10–26. https://doi.org/10.1111/gwat.12459

Jódar, J., Carpintero, E., Martos-Rosillo, S., Ruiz-Constán, A., Marín-Lechado, C., Cabrera-Arrabal, J. A., & González-Dugo, M. P. (2018). Combination of lumped hydrological and remote-sensing models to evaluate water resources in a semi-arid high altitude ungauged watershed of Sierra Nevada (Southern Spain). Science of The Total Environment, 625, 285–300. https://doi.org/10.1016/j.scitotenv.2017.12.300

Julander, R. P., Curtis, J., & Beard, A. (2007). The SNOTEL Temperature Dataset. Mountain Views. The Newsletter of the Consortium for Integrated Climate Research in Western Mountains, 1(2), 4–7.

Kampf, S. K., & Fassnacht, S. R. (2020). "Snow," Colorado Encyclopedia, last modified January 12, 2020, https://coloradoencyclopedia.org/article/snow.

Kattel, D. B., Yao, T., Yang, W., Gao, Y. & Tian, L. (2015). Comparison of temperature lapse rates from the northern to the southern slopes of the Himalayas. International Journal of Climatology, 35, 4431-4443. https://doi.org/10.1002/joc.4297

Khorchani, M., Vicente-Serrano, S. M., Azorin-Molina, C., Garcia, M., Martin-Hernandez, N., Peña-Gallardo, M., El Kenawy, A., & Domínguez-Castro, F. (2018).

Trends in LST over the peninsular Spain as derived from the AVHRR imagery data. Global and Planetary Change, 166, 75–93. https://doi.org/10.1016/j.gloplacha.2018.04.006

Kloog, I., Nordio, F., Coull, B. A., & Schwartz, J. (2014). Predicting Spatiotemporal Mean Air Temperature Using MODIS Satellite Surface Temperature Measurements across the Northeastern USA. Remote Sensing of Environment, 150, 132–139. https://doi.org/10.1016/j.rse.2014.04.024

Kyriakidis, P. C. (2004). A Geostatistical Framework for Area-to-Point Spatial Interpolation. Geographical Analysis, 36, 259–289. https://doi.org/10.1111/j.1538-4632.2004.tb01135.x

Li, Z. L., & Duan, S. B. (2018). Land Surface Temperature. Comprehensive Remote Sensing, 5, 264–283. https://doi.org/10.1016/B978-0-12-409548-9.10375-6

Li, Z. L., Tang, B. H., Hua. Wu, Ren, H., Yan, G., Wan, Z., Trigo, I. F., & Sobrino, J. A. (2013). Satellite-derived land surface temperature: current status and perspectives. Remote Sensing of Environment, 131, 14–37. https://doi.org/10.1016/j.rse.2012.12.008

Lookingbill, T. R., & Urban, D. L. (2003). Spatial estimation of air temperature differences for landscape-scale studies in montane environments. Agricultural and Forest Meteorology, 114(3-4), 141–151. https://doi.org/10.1016/S0168-1923(02)00196-X

Lundquist, J. D., & Huggett, B. (2008). Evergreen trees as inexpensive radiation shields for temperature sensors. Water Resources Research, 44, W00D04. https://doi.org/10.1029/2008WR006979

Ma., C. 2017. Evaluating and Correcting Sensor Change Artifacts in the SNOTEL Temperature Records, Southern Rocky Mountains (Master's thesis). Unpublished. Colorado: Watershed Science, Colorado State University, 43pp + 1 Appendix.

Ma, C., Fassnacht S. R., & Kampf S. K. (2019). How Temperature Sensor Change Affects Warming Trends and Modeling – An Evaluation across the State of Colorado. Water Resources Research, 55(11), 9748-9764. https://doi.org/10.1029/2019WR025921

Martin, T. C., Rocha, H. R., Joly, C. A., Freitas, H. C., Wanderley, R. L., & Silva, J.M. (2019). Fine-scale climate variability in a complex terrain basin using a high-resolution weather station network in southeastern Brazil. International Journal of Climatology, 39, 218–234. https://doi.org/10.1002/joc.5797

Martinec, J., Rango, A., Roberts, R. (1998). Snowmelt Runoff Model (SRM) user's manual. Geographica Bernensia P35, Department of Geography, University of Berne, 84pp.

Monestiez, P., Courault, D., Allard, D., & Ruget, F. (2001). Spatial interpolation of air temperature using environmental context: Application to a crop model. Environmental and Ecological Statistics, 8(4), 297–309. https://doi.org/10.1023/A:1012726317935

Naseer, A., Koike, T., Rasmy, M., Ushiyama, T., & Shrestha, M. (2019). Distributed hydrological modeling framework for quantitative and spatial bias correction for rainfall, snowfall, and mixed-phase precipitation using vertical profile of temperature. Journal of Geophysical Research: Atmospheres, 124, 4985–5009. https://doi.org/10.1029/2018JD029811

Natural Resources Conservation Service. (2016). NRCS: National Water and Climate Center SNOTEL data network. U.S. Department of Agriculture, available at: <https://www.wcc.nrcs.usda.gov/snow/ >, (last accessed: 05 February 2019)

Navarro-Serrano, F, López-Moreno, J. I., Azorin-Molina, C., Alonso-González, E., Tomás-Burguera, M., Sanmiguel-Vallelado, A., Revuelto, J., Vicente-Serrano, S. M. (2018). Estimation of near-surface air temperature lapse rates over continental Spain and its mountain areas. International Journal of Climatology, 38(8), 3233–3249. https://doi.org/10.1002/joc.5497

Navarro-Serrano, F., López-Moreno, J. I, Azorin-Molina, C., Buisán, S., Domínguez-Castro, F., Sanmiguel-Vallelado, A., Alonso-González, E., & Khorchani, M. (2019). Air temperature measurements using autonomous self-recording dataloggers in mountainous and snow covered areas. Atmospheric Research, 224, 168–179. https://doi.org/10.1016/j.atmosres.2019.03.034

Oyler, J. W., Dobrowski, S. Z., Ballantyne, A. P., Klene, A. E., & Running, S. W. (2015). Artificial amplification of warming trends across the mountains of the western United States, Geophysical Research Letters, 42, 153–161. https://doi.org/10.1002/2014GL062803

Pape, R., & Löffler, J. (2004). Modelling Spatio-Temporal Near-Surface Temperature Variation in High Mountain Landscapes. Ecological Modelling, 178, 483–501. https://doi.org/10.1016/j.ecolmodel.2004.02.019

Pepin, N. C., Daly, C., & Lundquist, J. (2011). The influence of surface versus free-air decoupling on temperature trend patterns in the western United States, Journal of Geophysical Research, 116, D10109. https://doi.org/10.1029/2010JD014769.

Rolland, C. (2003). Spatial and seasonal variations of air temperature lapse rates in alpine regions. Journal of Climate, 16(7), 1032–1046. https://doi.org/10.1175/1520-0442

Shiklomanov, A. I., Lammers, R. B., & Vörösmarty, C. J. (2002). Widespread decline in hydrological monitoring threatens Pan-Arctic Research. EOS Transactions, AGU, 83(2), 13–17. https://doi.org/10.1029/2002EO000007

Stewart, S.B., & Nitschke, C.R. (2017). Improving temperature interpolation using MODIS LST and local topography: a comparison of methods in south east Australia. Int. J. Climatol., 37: 3098-3110. https://doi.org/10.1002/joc.4902

Venable, N. B. H., Fassnacht, S. R., & Hendricks, A. D. (2015). Spatial changes in climate across Mongolia. In Proceedings of the Trans-Disciplinary Research Conference: Building Resilience of Mongolian Rangelands, Ulaanbaatar, Mongolia, 9–10 June 2015; Fernández-Giménez, M.E., Batkhishig, B., Fassnacht, S.R., Wilson, D., Eds.; Nutag Action and Research Institute: Ulaanbaatar, Mongolia, pp. 73–79.

Wang, L., Koike, T., Yang, K., & Yeh, P. J. -F. (2009). Assessment of a distributed biosphere hydrological model against MODIS land surface temperature and its

application in the upper Tone river basin. Journal of Hydrology, 377(1-2), 21–34. https://doi.org/10.1016/j.jhydrol.2009.08.005

Whiteman, C. D., Hubbe, J. M, & Shaw, W. J. (2000). Evaluation of an inexpensive temperature datalogger for meteorological applications. Journal of Atmospheric and Oceanic Technology, 17, 77–81. https://doi.org/10.1175/1520-0426(2000)017<0077:EOAITD>2.0.CO;2

Wrzesien, M., Pavelsky, T., Kapnick, S., Durand, M., Painter, T. (2015). Evaluation of snow cover fraction for regional climate simulations in the Sierra Nevada. International Journal of Climatology, 35(9), 2472–2484. https://doi.org/10.1002/joc.4136

Yang, Y. Z., Cai, W. H., & Yang, J. (2017). Evaluation of MODIS Land Surface Temperature Data to Estimate Near-Surface Air Temperature in Northeast China. Remote Sensing, 9, 410. https://doi.org/10.3390/rs9050410

Young, C. A., Escobar-Arias, M. I., Fernandes, M., Joyce, B., Kiparsky, M., Mount, J. F, Mehta, V. K., Purkey, D., Viers, J. H., & Yates, D. (2009). Modeling the Hydrology of Climate Change in California's Sierra Nevada for Subwatershed Scale Adaptation. Journal of the American Water Resources Association, 45(6), 1409-1423. https://doi.org/10.1111/j.1752-1688.2009.00375.x

Zhang, G. E., Yao, T., Xie, H., Qin, J., Ye, Q., Dai, Y., & Guo, R. (2014). Estimating surface temperature changes of lakes in the Tibetan Plateau using MODIS LST data. Journal of Geophysical Research: Atmospheres, 119, 8552–8567. https://doi.org/10.1002/2014JD021615

Zhang, Y. L., Li, X., Cheng, G. D., Jin, H. J., Yang, D. W., Flerchinger, G. N., et al. (2018). Influences of topographic shadows on the thermal and hydrological processes in a cold region mountainous watershed in northwest China. Journal of Advances in Modeling Earth Systems, 10, 1439– 1457. https://doi.org/10.1029/2017MS001264

Table 1. NSTGE for the SNOTEL stations, iButton network, MODIS estimates for SNOTEL pixels, and MODIS estimates for iButton pixels, for the daytime (7 am to 8 pm) and nighttime (the remaining time) periods calculated as the average of the hourly NSTGE which have associated a R^2 above the considered thresholds.

	NSTGE (°C km^{-1}) coarse resolution - SNOTEL stations		NSTGE (°C m^{-1}) fine resolution - iButton sensors		NSTGE (°C km^{-1}) coarse resolution - MODIS pixels		NSTGE (°C m^{-1}) fine resolution - MODIS pixels	
R^2 threshold	daytime	nighttime	daytime	nighttime	daytime	nighttime	daytime	nighttime
none	-0.0068	--0.0047	0.0394	0.0984	-0.0074	-0.0045	-0.0346	0.0047
0.1	-0.0076	-0.0060	0.0485	0.1147	-0.0117	-0.0047	-0.0372	0.0058
0.2	-0.0078	-0.0065	0.0573	0.1227	-0.0139	-0.0049	-0.0408	0.0076
0.3	-0.0080	-0.0067	0.0668	0.1275	-0.0194	-0.0048	-0.0456	0.0077
0.4	-0.0082	--0.0067	0.0733	0.1332	-0.0276	-0.0037	-0.0475	0.0087

Intra-day variability of temperature and its near-surface gradient with elevation over mountainous terrain: comparing MODIS Land Surface Temperature data with coarse and fine scale near-surface measurements

Antonio-Juan Collados-Lara *, Steven R. Fassnacht, David Pulido-Velazquez, Anna K.D. Pfohl, Enrique Morán-Tejeda, Niah B.H. Venable, Eulogio Pardo-Igúzquiza, and Kira Puntenney-Desmond

* Corresponding author

This work assesses the variability of near-surface temperature at two scales in the same mountain region (SNOTEL measurements are employed for coarse scale and iButton measurements for fine scale) and compares them to MODIS land surface temperature.

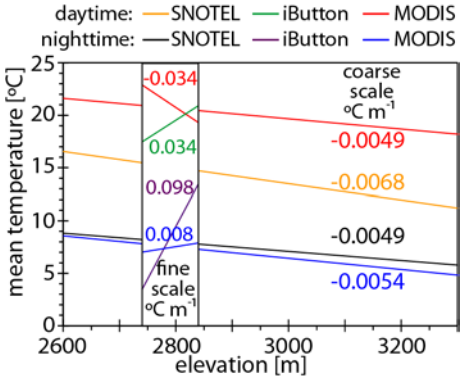

Significant differences in the temperature patterns are observed in the measurements at the two scales (e.g. at the fine scale an inverse gradient of temperature with elevation is observed). MODIS also shows differences with both measurements in terms of mean, standard deviation and temperature gradients with elevation.

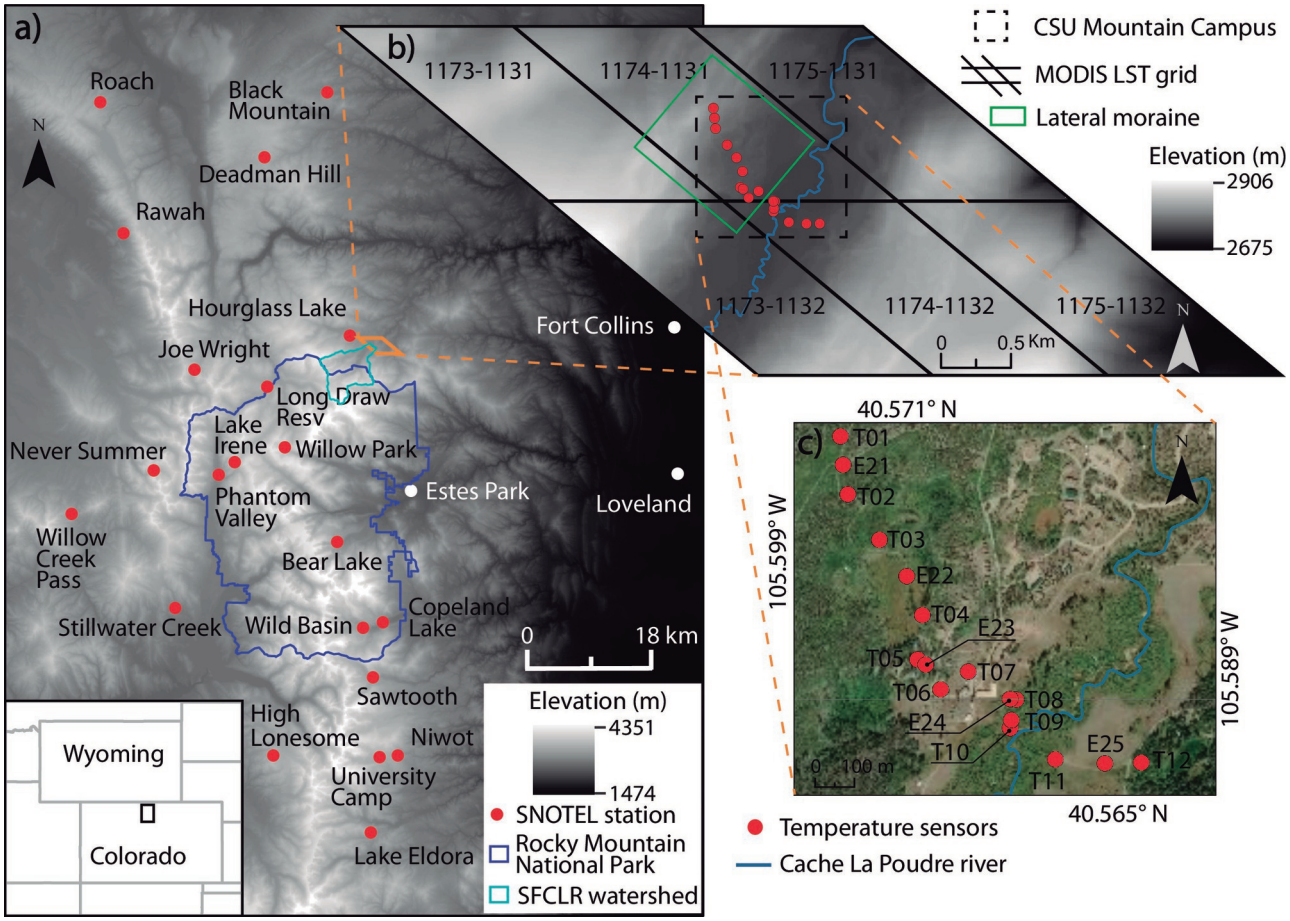

joc_6778_joc-20-0413_r3_figure1.eps

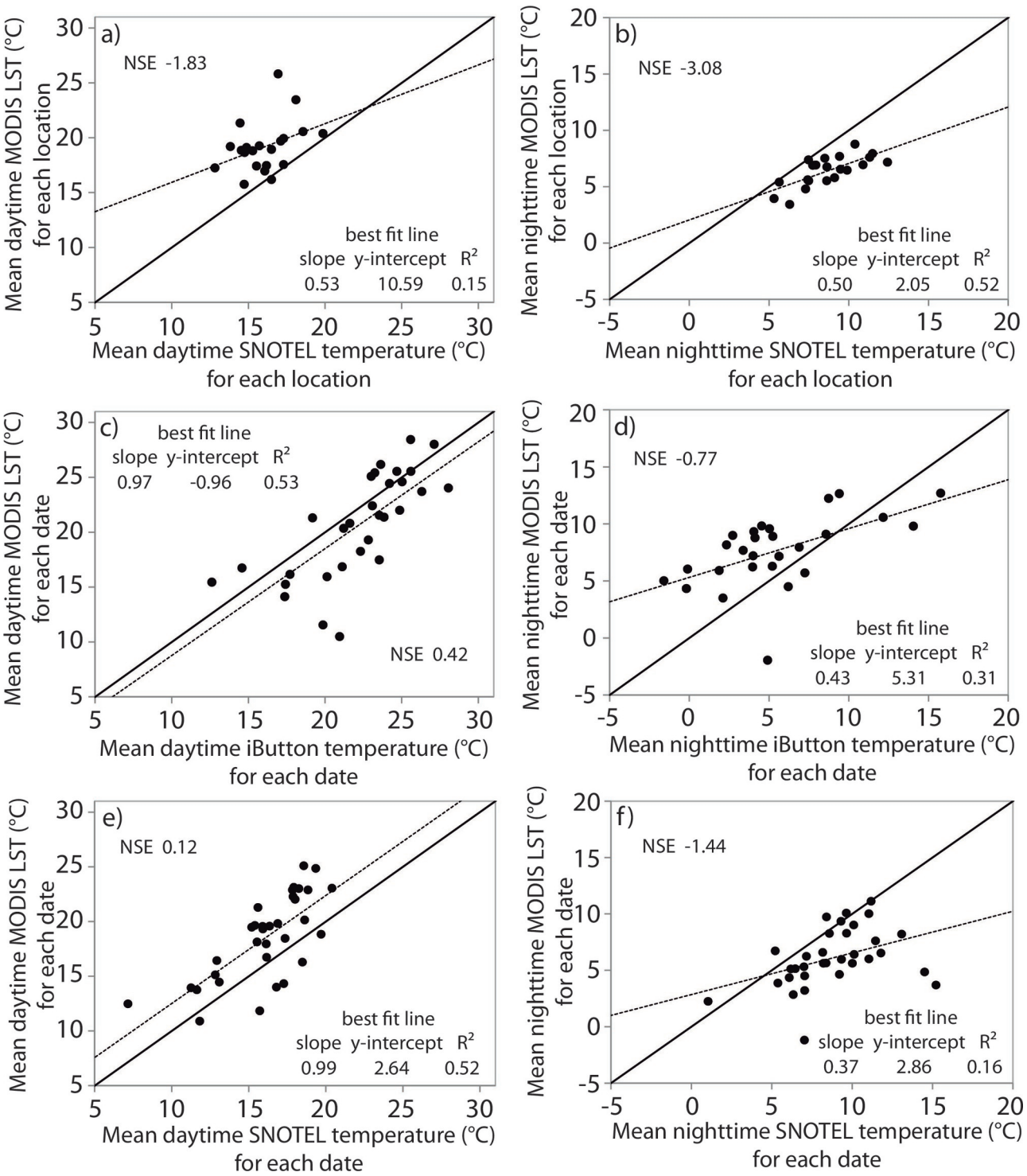

joc_6778_joc-20-0413_r3_figure2.eps

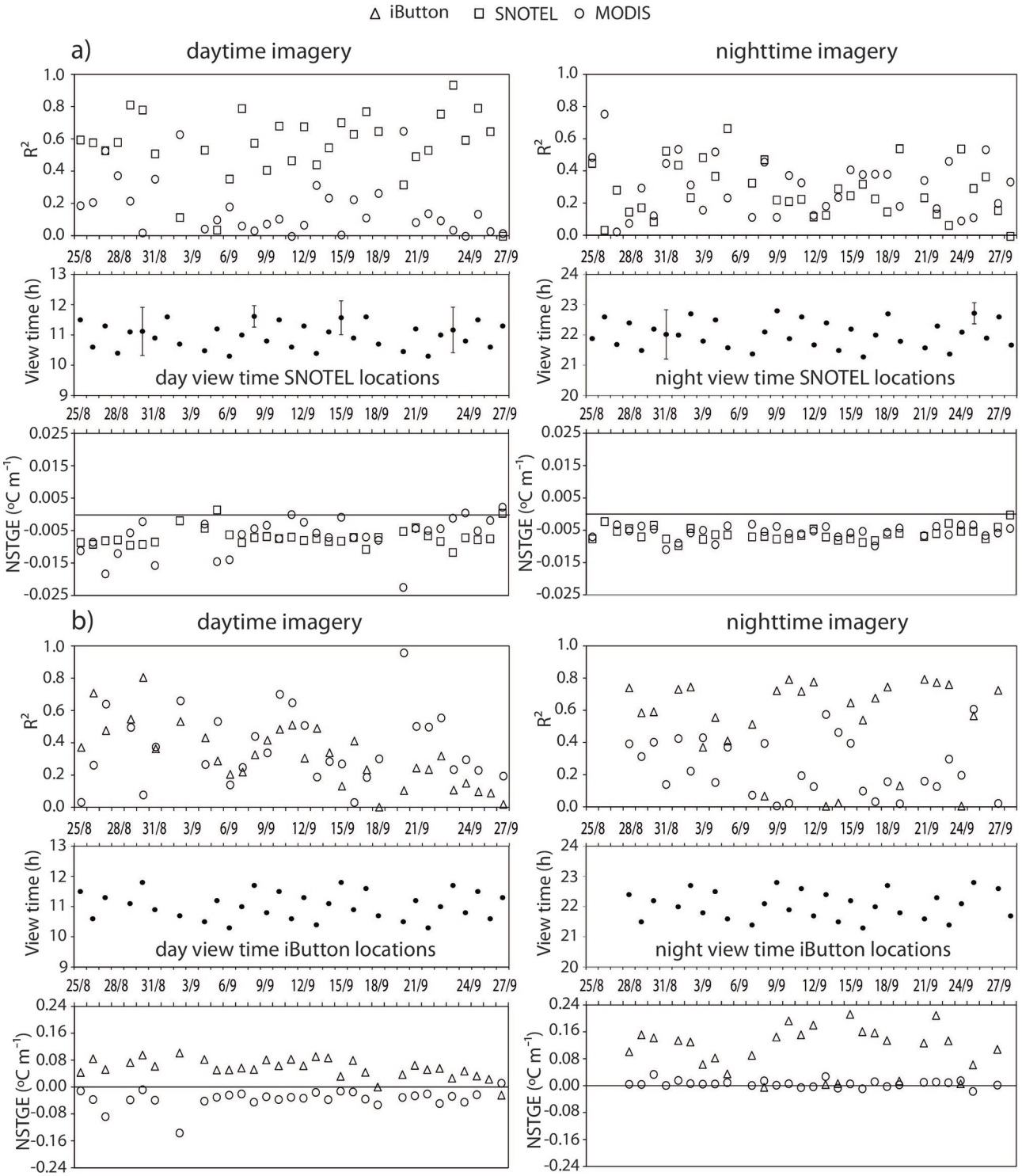

joc_6778_joc-20-0413_r3_figure3.eps

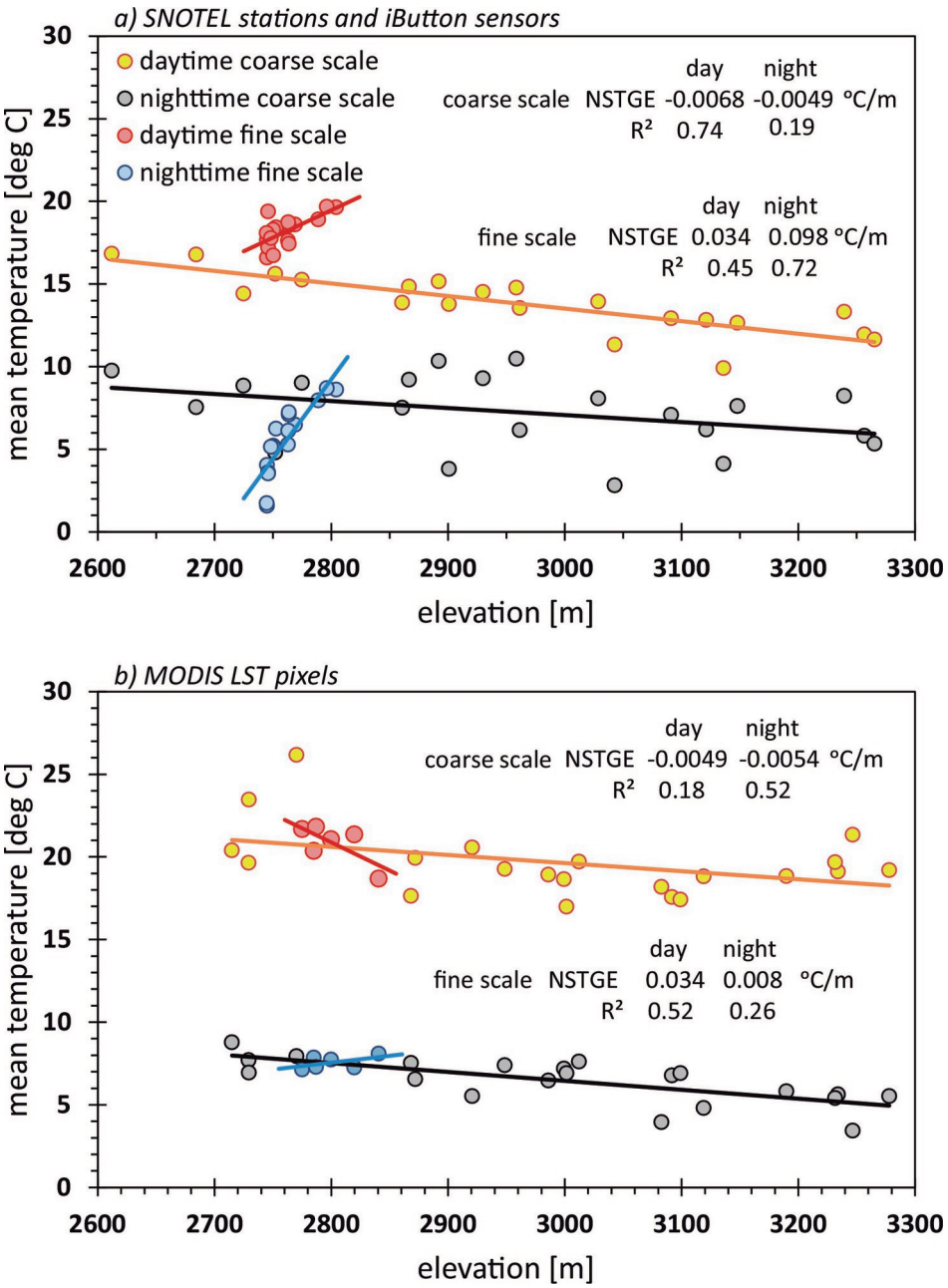

joc_6778_joc-20-0413_r3_figure4.eps

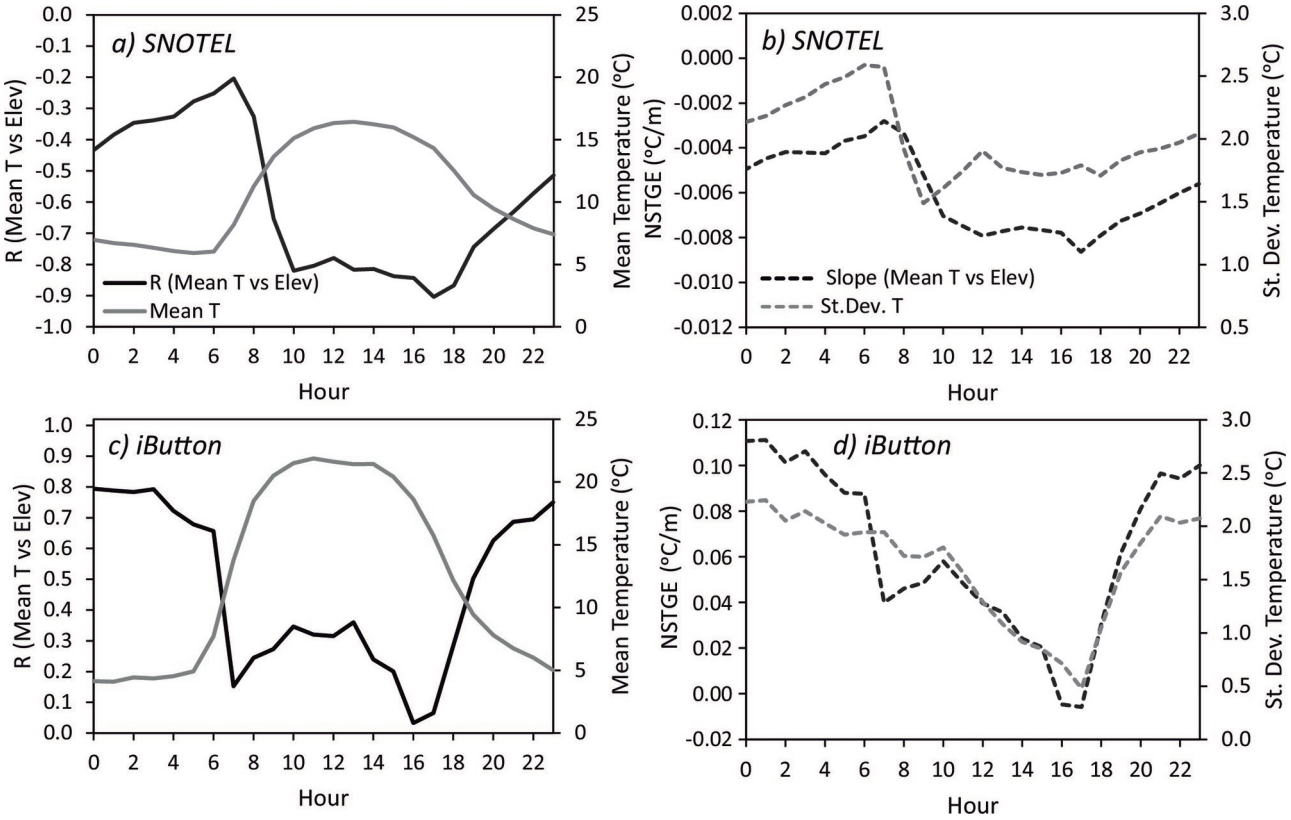

joc_6778_joc-20-0413_r3_figure5.eps

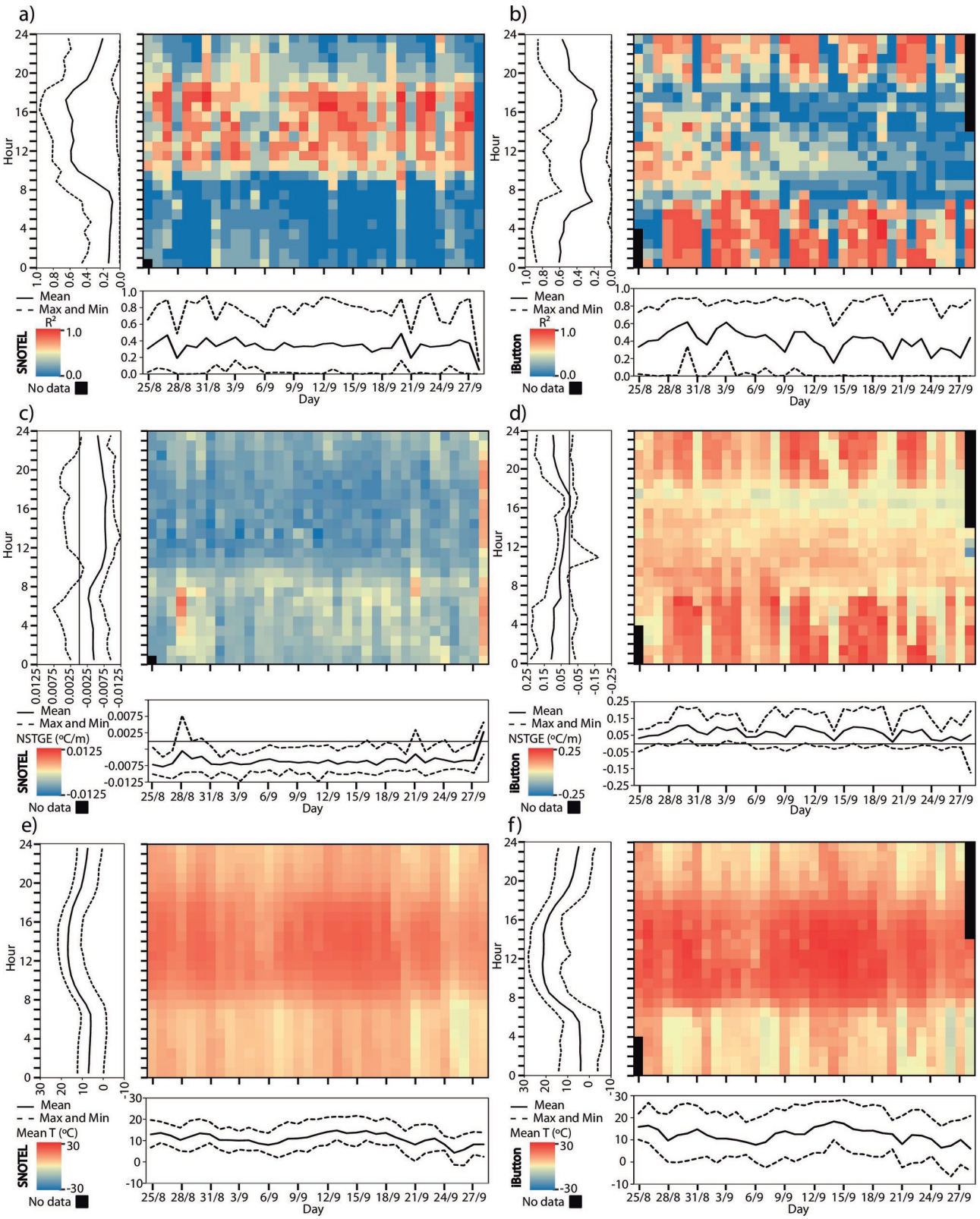

joc_6778_joc-20-0413_r3_figure6.eps

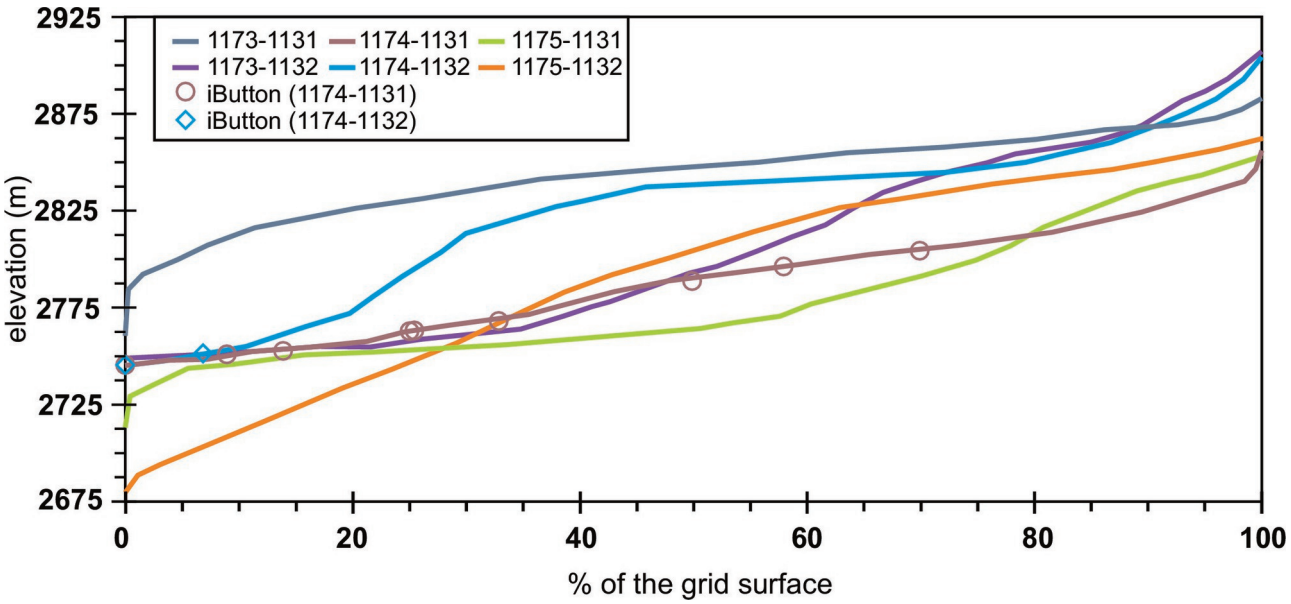

joc_6778_joc-20-0413_r3_figures1.eps

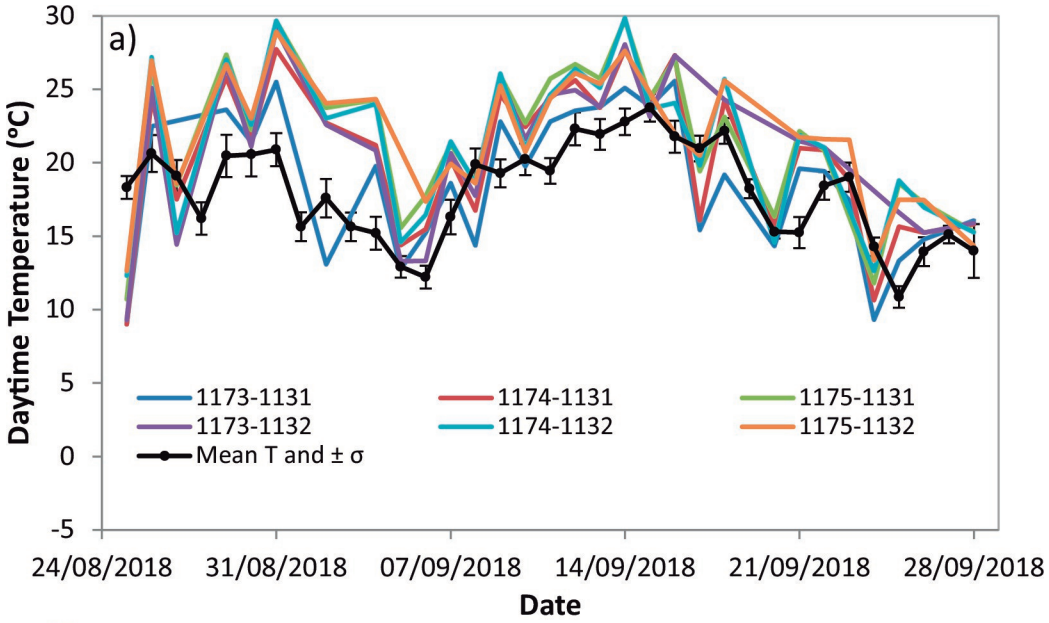

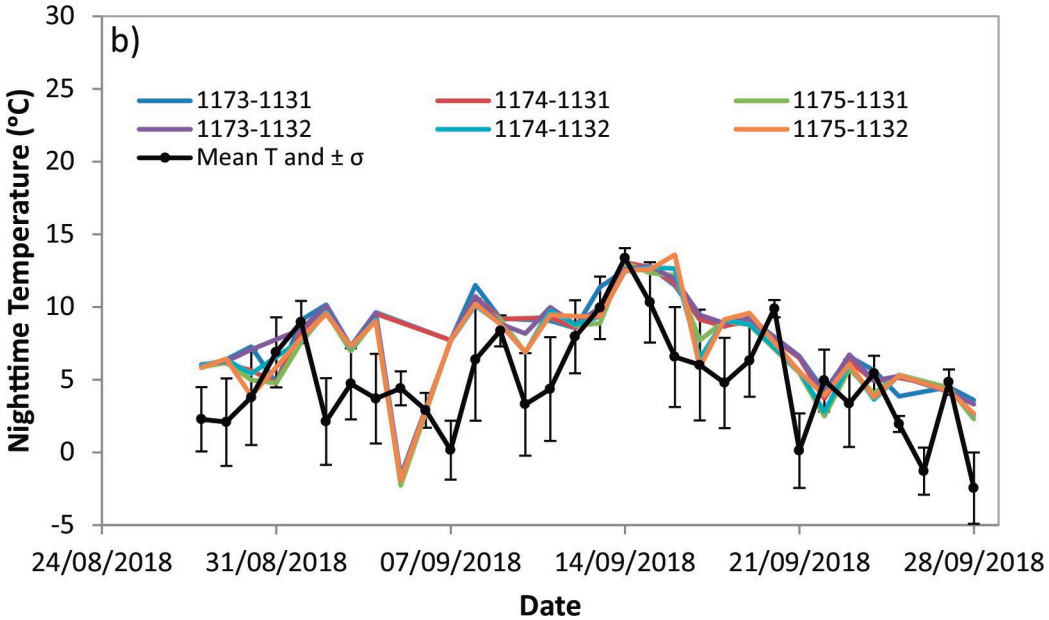

joc_6778_joc-20-0413_r3_figures2.eps

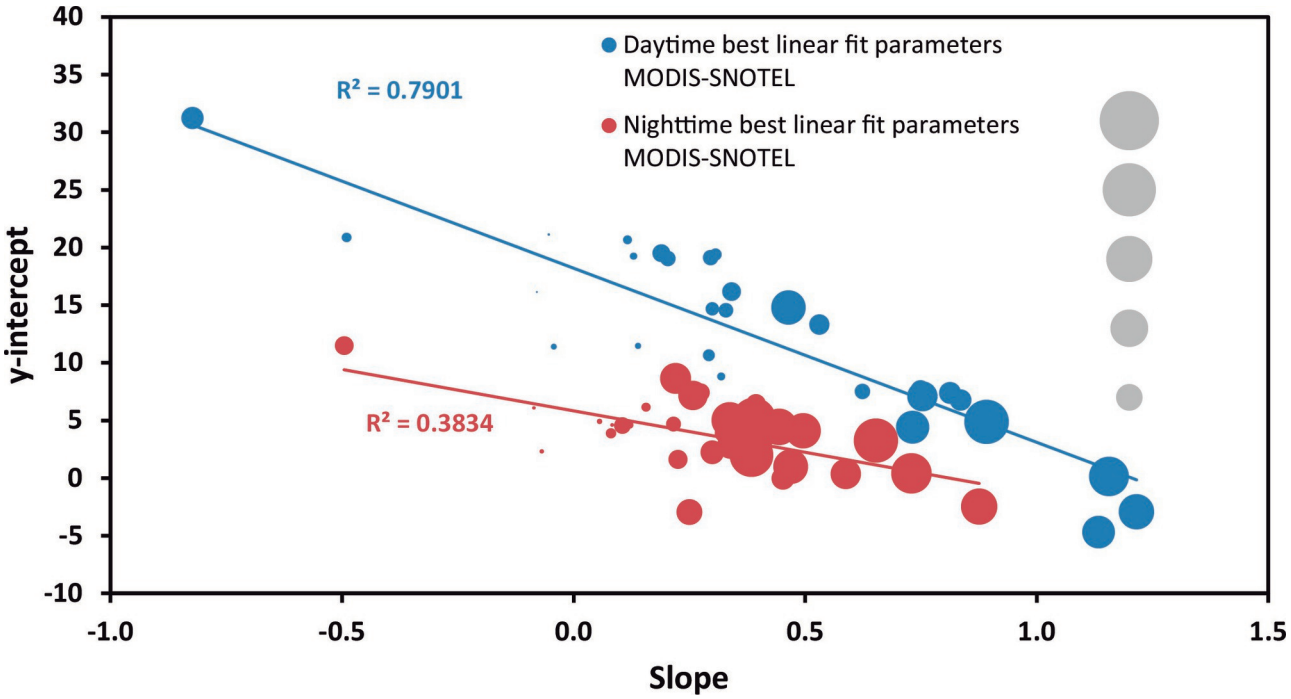

joc_6778_joc-20-0413_r3_figures3.eps

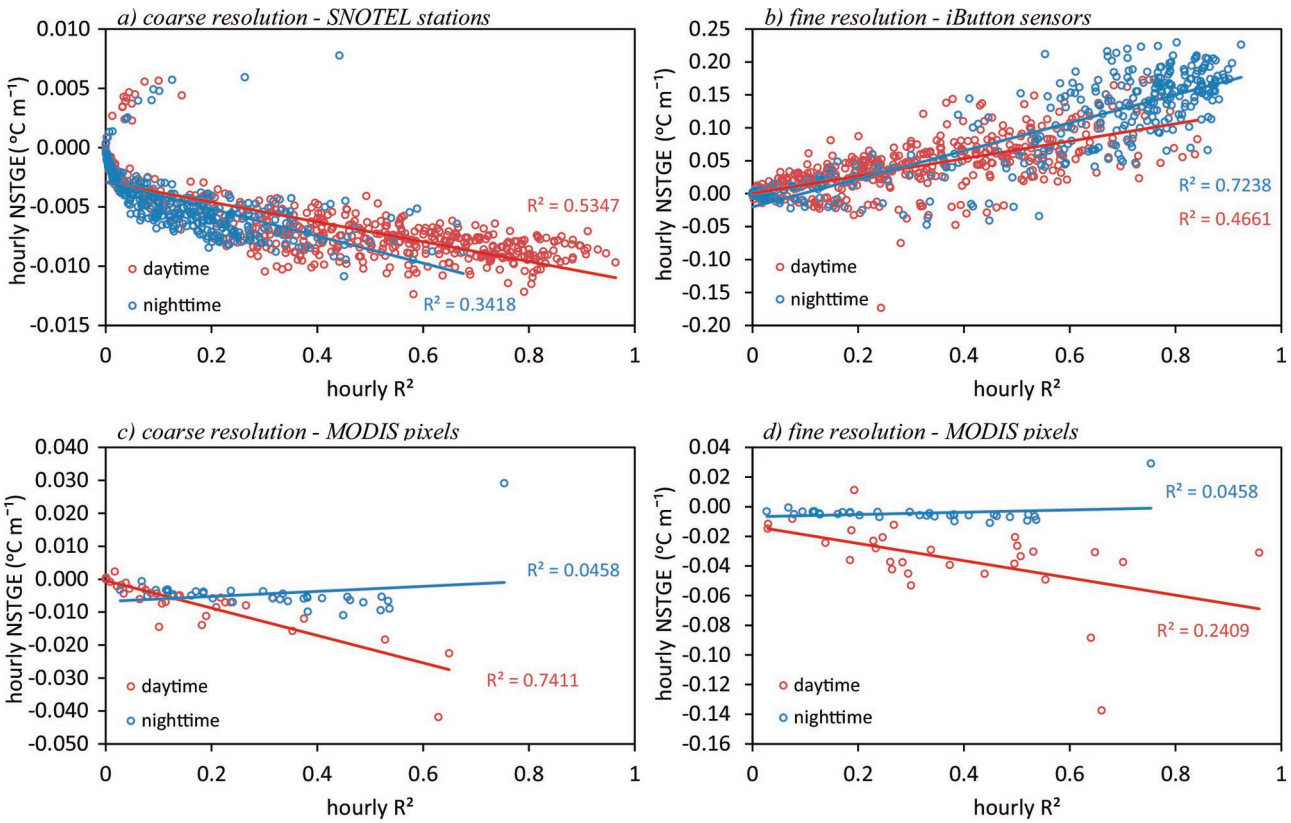

joc_6778_joc-20-0413_r3_figures4.eps

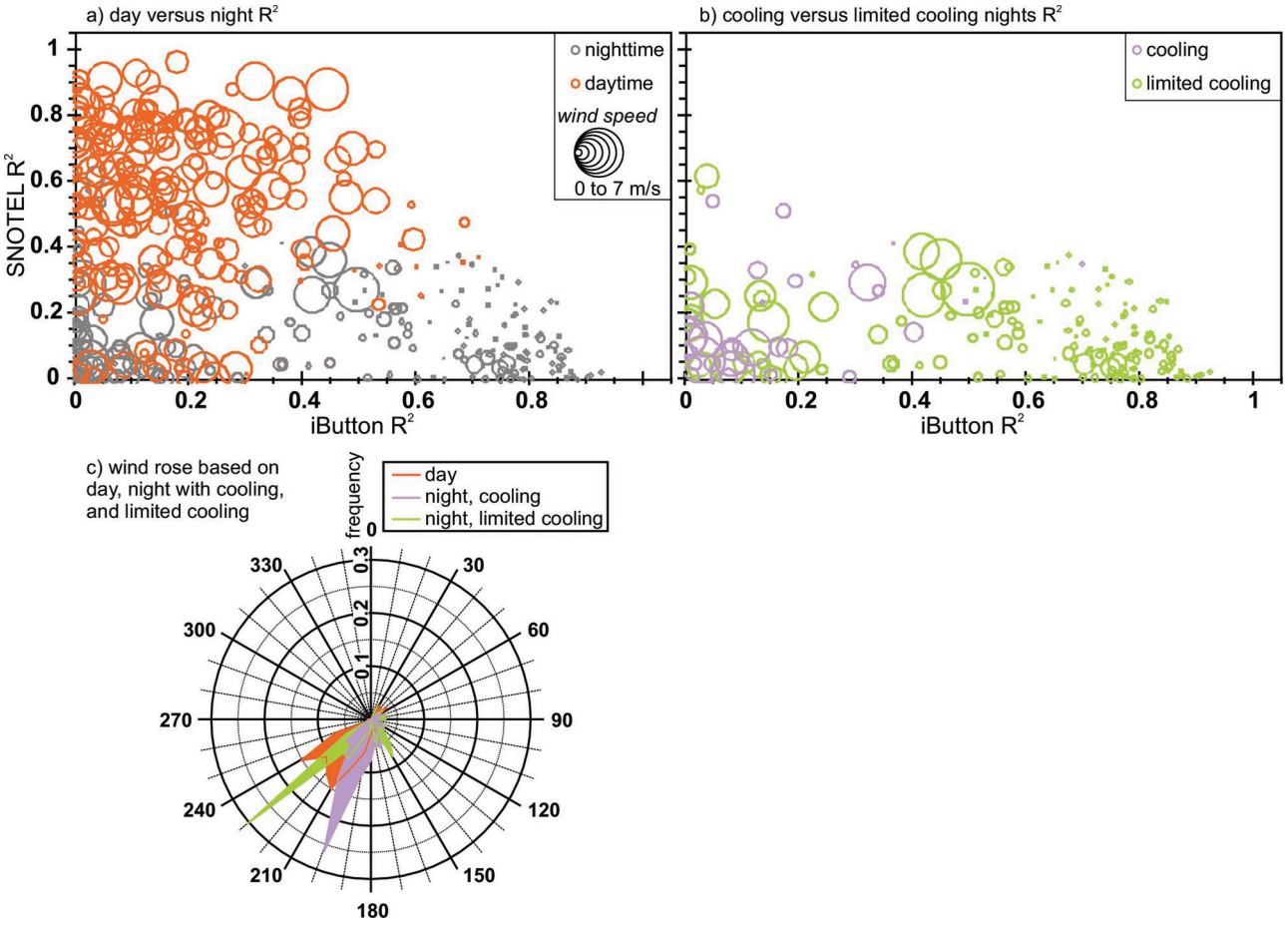

joc_6778_joc-20-0413_r3_figures5.eps

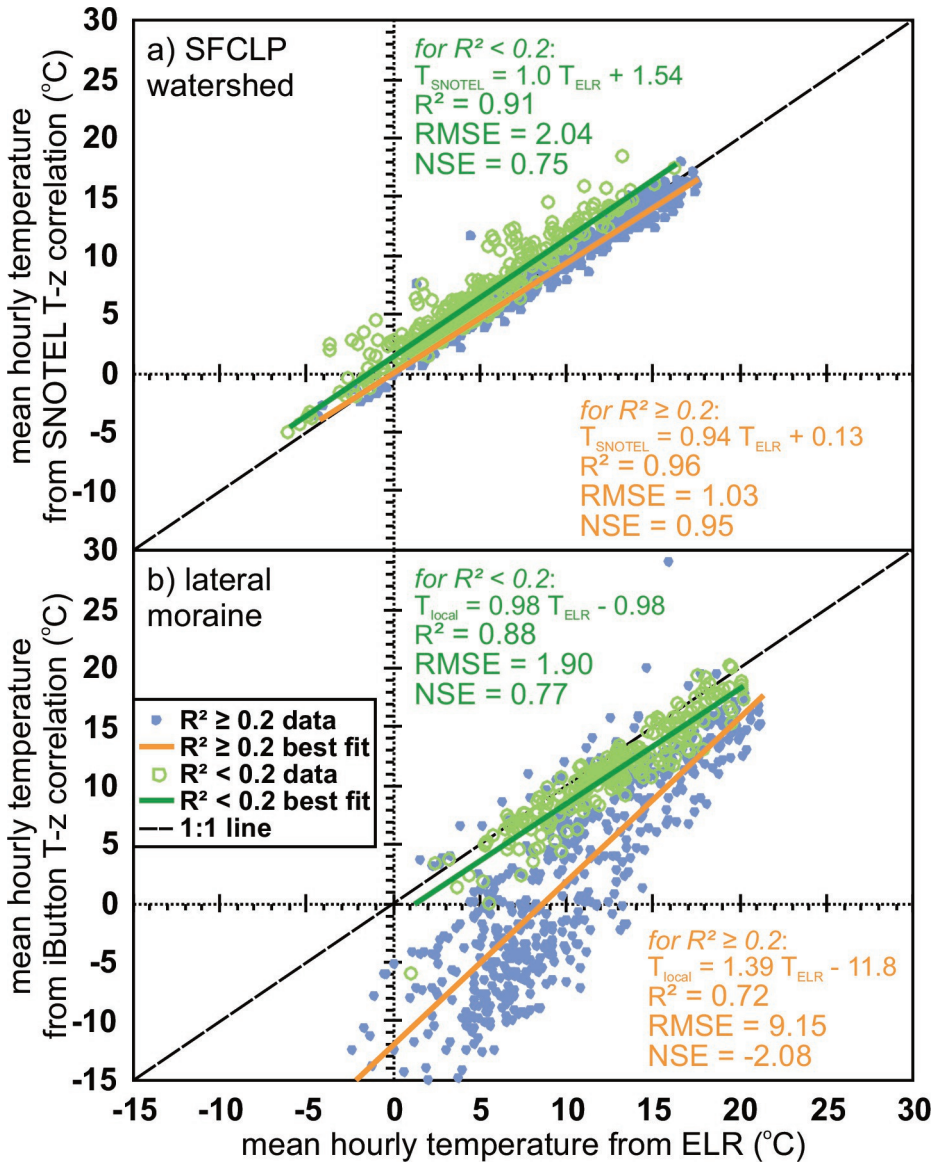

joc_6778_joc-20-0413_r3_figures6.eps

Intra-day variability of temperature and its near-surface gradient with elevation over mountainous terrain: comparing MODIS Land Surface Temperature data with coarse and fine scale near-surface measurements

Antonio-Juan Collados-Lara *, Steven R. Fassnacht, David Pulido-Velazquez, Anna K.D. Pfohl, Enrique Morán-Tejeda, Niah B.H. Venable, Eulogio Pardo-Igúzquiza, and Kira Puntenney-Desmond

* Corresponding author

This work assesses the variability of near-surface temperature at two scales in the same mountain region (SNOTEL measurements are employed for coarse scale and iButton measurements for fine scale) and compares them to MODIS land surface temperature. Significant differences in the temperature patterns are observed in the measurements at the two scales (e.g. at the fine scale an inverse gradient of temperature with elevation is observed). MODIS also shows differences with both measurements in terms of mean, standard deviation and temperature gradients with elevation.

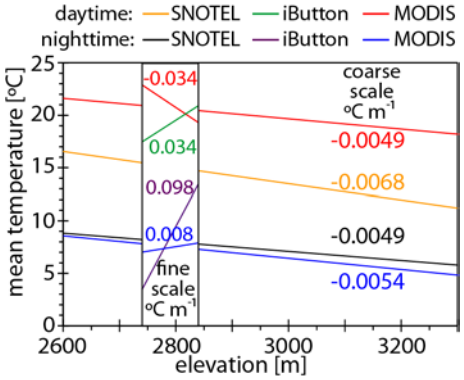

Table 1. NSTGE for the SNOTEL stations, iButton network, MODIS estimates for SNOTEL pixels, and MODIS estimates for iButton pixels, for the daytime (7 am to 8 pm) and nighttime (the remaining time) periods calculated as the average of the hourly NSTGE which have associated a R^2 above the considered thresholds.

	NSTGE (°C km^{-1}) coarse resolution - SNOTEL stations		NSTGE (°C m^{-1}) fine resolution - iButton sensors		NSTGE (°C km^{-1}) coarse resolution - MODIS pixels		NSTGE (°C m^{-1}) fine resolution - MODIS pixels	
R^2 threshold	daytime	nighttime	daytime	nighttime	daytime	nighttime	daytime	nighttime
none	-0.0068	--0.0047	0.0394	0.0984	-0.0074	-0.0045	-0.0346	0.0047
0.1	-0.0076	-0.0060	0.0485	0.1147	-0.0117	-0.0047	-0.0372	0.0058
0.2	-0.0078	-0.0065	0.0573	0.1227	-0.0139	-0.0049	-0.0408	0.0076
0.3	-0.0080	-0.0067	0.0668	0.1275	-0.0194	-0.0048	-0.0456	0.0077
0.4	-0.0082	--0.0067	0.0733	0.1332	-0.0276	-0.0037	-0.0475	0.0087